Macroscopic quantum fluctuations of pulsed nanosecond optical parametric generation in periodically-poled $LiNbO_3$

Yiyi Guan,* Joseph W. Haus, and Peter Powers
Electro-Optics Program, University of Dayton, 300 College Park, Dayton, Ohio 45469-0245, USA
(Received 9 March 2004; published 15 February 2005)

We present simulations and experimental results for quantum-noise-initiated emission from an optical parametric generator (OPG) fabricated from periodically poled lithium niobate. The model we employ, which includes transverse coupling effects to enable off-axis phase matching, has been successfully used for describing broadband emission spectra in OPG's and optical parametric amplifiers. The emission spectra and the quantum statistics deduced from macroscopic fluctuations are compared between simulations and experiment.

DOI: 10.1103/PhysRevA.71.023809 PACS number(s): 42.65.−k, 42.50.Lc, 42.50.Ct, 42.50.Fx

I. INTRODUCTION

The signals from optical parametric generators (OPG's) and optical parametric oscillators (OPO's) are initiated from spontaneous parametric emission. Louisell *et al.* [1] explored the properties of quantum fluctuations in the output signal and idler fields of the parametric amplifier using a single-mode model. The quantum fluctuations in the initial field lead to macroscopic quantum fluctuations in the OPG output and during the initial start-up of the OPO. Many researchers have studied the quantum optical properties of OPO's, such as statistical properties of the OPO emission [2], fluctuations of the difference between the signal and idler intensity in the nondegenerate OPO [3], or fluctuations in the OPO energy and spectra [4,5]. The above quantum optical studies were based on plane-wave models, and the pump wave is also single mode. Arisholm introduced a simulation model for the OPO that includes multiple longitudinal modes and multiple transverse modes [6]. In his model, the OPO modes are determined by the parametric gain bandwidth, the spectral and spatial properties of the pump beam, and the OPO cavity. Multimode descriptions of OPO's can be found in the literature [7], and recent papers have discussed temporal modes and their coherence properties (see, for instance, Ref. [8] and references therein).

An OPG has the same optical parametric amplification process as an OPO except it does not have a cavity. So they share some common characteristics—for instance, the same quantum noise initiation and phase matching conditions. However, the OPG is a single-pass parametric process; therefore, it is expected to have features that are similar to other single-pass stimulated optical amplification processes, such as superfluorescence [9,10], amplified spontaneous emission [11], and stimulated Raman scattering (SRS) [12–14]. In these processes, the initial spontaneous noise is amplified to a macroscopic level in a gain medium without a cavity.

For instance, the quantum fluctuations for Raman amplifiers have been extensively studied. Walmsley and Raymer elucidated the spatial and temporal coherent properties of SRS and the macroscopic quantum fluctuations of Stokes pulse energy, both experimentally [15] and theoretically [16]. Experiments confirmed that the shape of the probability distribution of the Stokes pulse energy is determined by the amount of both temporal incoherence and spatial incoherence. When a single mode is excited, the intensity distribution function will be approximately an exponential function; as more independent modes are excited, the distribution function will tend toward a Gaussian, as expected from the central-limit theorem. The transient SRS (with a single temporal mode) with large Fresnel number and interaction volume is a gain-guided amplifier, which is classified as a non-Hermitian optical system [17,18]. For instance, the transverse eigenmodes (spatial modes) of a gain-guided Raman amplifier are biorthogonal and correlated, which causes beam-pointing fluctuations [19]. The statistics of the beams, therefore, provides important observations of the quantum nature of the emission process; other observations, such as the macroscopic fluctuations of the output Stokes pulse energy, also reflect the quantum nature of their origin.

The spatial statistics due to the quantum optical properties of OPG's has not been reported in the literature so far. To better understand this process we use quasi-phase-matching (QPM) crystal pumped by a nanosecond-pulsed $Nd:YVO_4$ laser to generate efficient infrared light by optical parametric generation [20–25]. In this paper, we examine both theoretically and experimentally the quantum noise initiation in OPG's, the power probability distribution function of individual modes, and the total energy probability distribution function of OPG pulses. Both undepleted and depleted pump cases will be quantified through our simulations. For the undepleted pump case with constant transverse pump profile, an analytical solution of coupled-mode wave equations is available [26]; for the depleted pump case, a numerical model is used to simulate the dynamical evolution of the fields. In Sec. II, the quantum noise initiation is discussed and our numerical model is introduced. Both experimental and numerical results are displayed in Sec. III. Comparison between experiment and calculations is discussed in Sec. IV.

II. QUANTUM NOISE INITIATION AND NUMERICAL MODEL

The OPG is a high-gain amplification process that is initiated by spontaneous parametric emission of signal and idler

*Electronic mail: guanyiyiz@notes.udayton.edu

photons. Since the emission is a quantum noise process, it endows the output fields with fluctuations that are characteristic of the underlying vacuum fields. As mentioned above, the quantum noise initiation of the OPG is the same as for OPO's, which has been discussed in several publications [5,6]. In the vacuum state, the amplitude and phase of initial electromagnetic fields have a Gaussian random distribution. The electrical field operator is decomposed into positive and negative frequency contributions as

$$E(\vec{r},t) = E^{(+)}(\vec{r},t) + E^{(-)}(\vec{r},t), \tag{1}$$

where the positive frequency component of the electric field is

$$E^{(+)}(\vec{r},t) = \sum_l \varepsilon_l a_l e^{i(\vec{k}_l\cdot\vec{r}-\omega_l t)} \tag{2}$$

and the negative frequency component is

$$E^{(-)}(\vec{r},t) = \sum_l \varepsilon_l^* a_l^\dagger e^{i(-\vec{k}_l\cdot\vec{r}+\omega_l t)}. \tag{3}$$

The equal-time creation and annihilation operators $\{a_l^\dagger, a_l\}$ satisfy the commutation relations

$$[a_l, a_{l'}^\dagger] = \delta_{ll'}. \tag{4}$$

The coefficient under the summation has the value

$$\varepsilon_l = \sqrt{\frac{\hbar\omega_l}{2\epsilon_0 V}}. \tag{5}$$

Here, V is a quantization volume.

The field quantization leads to average of the anti-normal-ordered, equal-time operators expressed as

$$\langle E^+(\vec{r},t)E^-(\vec{r}',t)\rangle = \frac{\hbar\omega}{2\epsilon_0}\delta(\vec{r}-\vec{r}'). \tag{6}$$

The average initial electric field is zero. When the volume is discretized the equal-time variance of initial electrical field is given by

$$\langle E^+(\vec{r},t)E^-(\vec{r},t)\rangle = \frac{\varepsilon_l^2 V}{\Delta V} = \frac{\hbar\omega}{2\epsilon_0\Delta V}, \tag{7}$$

where ΔV is the volume of a unit cell in our lattice. ω is the center frequency of the electric field. In the coherent-state representation, the field operators are replaced by complex field functions whose variance is given by the above expression:

$$\langle |E(\vec{r},t)|^2\rangle = \frac{\hbar\omega}{2\epsilon_0\Delta V}. \tag{8}$$

A Gaussian random number generator is used to generate a complex random value with zero mean and the variance of $\hbar\omega/2\epsilon_0\Delta V$ for each mode (including frequency modes and their transverse modes). In order to include phase fluctuations in the initial field, the random value is a complex number. The volume element radiates the field into 4π steradians, and the amplification is restricted to a small angular acceptance determined by the pump beam profile and the length of the amplifier medium.

There are two stages in the signal amplification process: the quantum stage and the classical stage. In the quantum stage, no external signal and idler field seeds the process, the pump is treated as undepleted, and the quantum noise dominates the initiation process. The conversion to classical equations (here we implicitly treat antinormal operator ordering) is exact in the linear regime, because linear equations are the same whether quantum mechanical or classical and thus they have identical solutions. As a simple example consider the harmonic oscillator model. The classical and quantum mechanical solutions of the equations of motion (Heisenberg equations of motion or Newton equations of motion) are identical. However, in the nonlinear regime the field amplitudes are large enough that the fields can be described classically. This is the same theoretical approach that is used for superfluorescence or for stimulated Raman scattering. In the OPG when the signal grows to a high level, the process crosses over to the classical stage and the subsequent dynamics can be treated classically, then the background quantum noise is negligible. For both stages, the propagation equations of the fields are the same, except that the operators are used in quantum stage. In fact, we can treat the whole process classically by taking the quantum noise as our initial signal field, which is a similar approach used for OPO's [6].

As we mentioned above, OPG amplification is similar to Raman-Stokes amplification; however, the phase-matching condition is automatically satisfied in Raman-Stokes amplification [26]. Unlike SRS, OPG amplification requires phase-matching conditions. In the OPG process, a pump wave of frequency ω_p propagates through a nonlinear medium and generates two waves (the signal and idler) at frequencies ω_s and ω_i. According to the energy conservation relation, they satisfy

$$\omega_p = \omega_s + \omega_i. \tag{9}$$

Many signal-idler pairs are generated for a given pump wave, but the conversion efficiency of each pair is limited by its wave vector mismatch, which for the QPM interaction is

$$\Delta\vec{k} = \vec{k}_p - \vec{k}_s - \vec{k}_i - \vec{k}_g, \tag{10}$$

where the subscripts p, s, and i refer to the pump, signal, and idler wave vectors, respectively. $\vec{k}_g = \hat{e}_z 2\pi/\Lambda$ is the wave vector of the dipole grating used for QPM, where the direction of the grating is along the z axis (i.e., the unit vector $\hat{e}_z$) and Λ is the grating period. When $\Delta\vec{k}=0$ the phase matching is perfect; in this case, the crystal has the biggest amplification efficiency for that signal-idler pair. Like Stokes-anti-Stokes coupling in SRS [26], perfect phase matching can always be achieved if the signal wave propagates at some nonzero angle with respect to the pump wave, which is called off-axis phase matching. In a previous paper [27], we examined the off-axis phase matching result, which together with a broad transverse pump profile can yield a broad spectral band for the signal wave in an elliptical pump beam.

Since the maximum noncollinear phase-matching angle is around 3°, the paraxial approximation is still valid. In this model, since we use a small pump beam, the angle turns out to be below 1°. Each signal-idler pair can be regarded as a

distinct mode, and its dynamics during propagation chooses a direction with perfect phase matching. We study the OPG process for a long pump pulse (several nanoseconds), so we assume that the pump wave is a single frequency with a simple Gaussian transverse profile. Also, at any moment the pump is quasi-cw inside the medium. Our numerical model is $(2N+1)$ equations, which accounts N pairs of signal and idler longitudinal modes plus one pump mode. The coupled-mode equations are written in the form

$$\frac{\partial \tilde{E}_{sn}(\omega_{sn},x,z)}{\partial z} - \frac{i}{2k_{sn}}\nabla_{\perp}^{2}\tilde{E}_{sn}(\omega_{sn},x,z) = i\frac{\omega_{sn}\chi^{(2)}}{2n_{sn}c}\tilde{E}_{p}(\omega_{p},x,z)\tilde{E}_{in}^{*}(\omega_{in},x,z)e^{(i\Delta k_{n}z)}, \quad (11)$$

$$\frac{\partial \tilde{E}_{in}(\omega_{in},x,z)}{\partial z} - \frac{i}{2k_{in}}\nabla_{\perp}^{2}\tilde{E}_{in}(\omega_{in},x,z) = i\frac{\omega_{in}\chi^{(2)}}{2n_{in}c}\tilde{E}_{p}(\omega_{p},x,z)\tilde{E}_{sn}^{*}(\omega_{sn},x,z)e^{(i\Delta k_{n}z)}, \quad (12)$$

$$\frac{\partial \tilde{E}_{p}(\omega_{p},x,z)}{\partial z} - \frac{i}{2k_{p}}\nabla_{\perp}^{2}\tilde{E}_{p}(\omega_{p},x,z) = i\frac{\omega_{p}\chi^{(2)}}{2n_{p}c}\sum \tilde{E}_{sn}(\omega_{sn},x,z)\tilde{E}_{in}(\omega_{in},x,z)e^{(-i\Delta k_{n}z)}, \quad (13)$$

where the subscript n denotes a particular frequency mode. In our model, we only consider one transverse dimension; we expect that the result for two dimensions will be similar. For each frequency mode, the transverse spatial intensity of output signal wave is determined by its off-axis phase matching angle and spatial properties of the gain area, so that each frequency mode has its own multi-transverse-mode spectrum. The diffraction term enables off-axis phase matching in our model and also allows us to simply account for the transverse modes. This model gave us very good results in describing the broadband spectra of the signal wave in the elliptical pumped OPG [27]. We apply this model here to study the statistical properties of nanosecond OPG pulses. In our calculations, the pump pulse is divided into 20 equal-time intervals, which is sufficient for describing the different pump levels in a single pulse. The power spectrum of the OPG signal is the summation of the output signal from each pump pulse segment in the far field.

III. EXPERIMENTAL AND NUMERICAL ANALYSIS OF THE SPECTRAL FLUCTUATIONS

A. Experimental results

The experimental setup is similar to that described in Refs. [28,29]; an output facet from the crystal is polished at Brewster's angle in the vertical direction to suppress étalon effects. A QPM lithium niobate crystal is used as the nonlinear medium, and the sample length is 3 cm and its height is 1 mm. Due to the effects of transverse pump beam size on the signal spectra bandwidth [27], we use a narrow pump beam of 400 μm diameter and the output signal spectra is a narrow band around the on-axis phase-matching mode wavelength. The pump source is an injection-seeded Nd:YVO_4 laser, which operates at a wavelength of 1.064 μm and has a repetition rate of 883 Hz and a pulse width of 3.5 ns. The spectrometer resolution is 0.3 cm^{-1} (0.07 nm). We measured the signal spectra in the far field and recorded the mode intensity fluctuations from pulse to pulse. The data were collected from a set of pulses, which was used to examine the statistical properties of individual mode intensities, and the pulse intensity averaged over all the modes of OPG pumped at various energy levels. In this paper the pump threshold is defined as the pump pulse energy for which the signal is detectable; with our detector, this corresponds to approximately 1 μJ of energy.

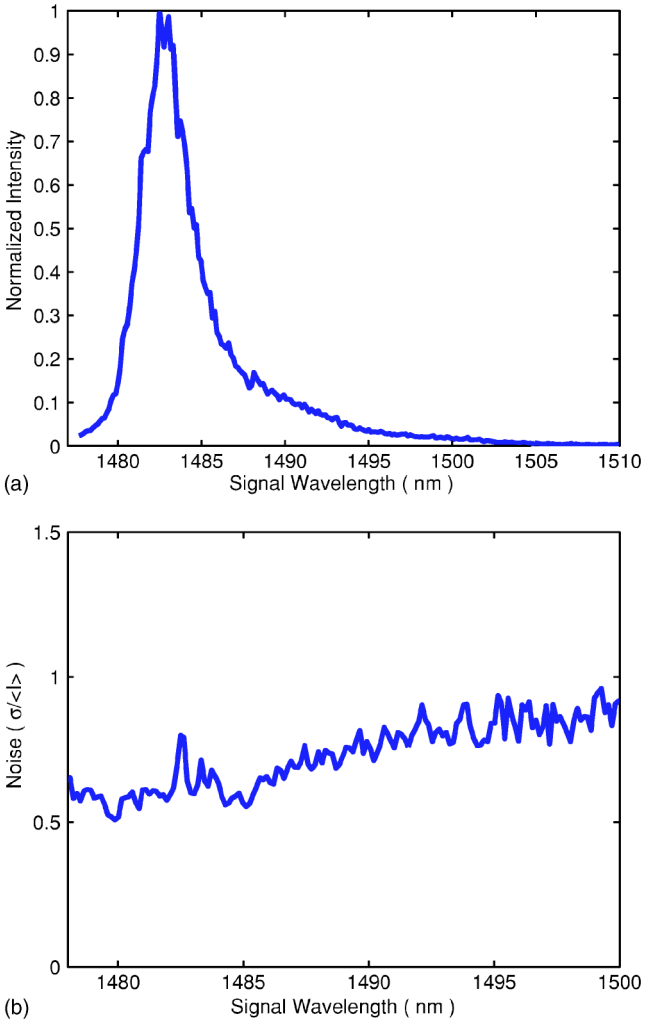

FIG. 1. Experimental results for the OPG pumped at 2 times above the threshold energy: (a) mode spectrum of the signal wave calculated by averaging over 300 output pulses and (b) noise level of individual modes calculated by averaging over 300 output pulses.

Figure 1(a) is the measured signal spectra averaged over 300 pulses. The OPG is pumped at 2 times threshold. Figure 1(b) is a plot of the measured intensity noise of individual modes of OPG, also pumped at 2 times threshold. The fluctuations are higher for the modes in the wings of the spectral

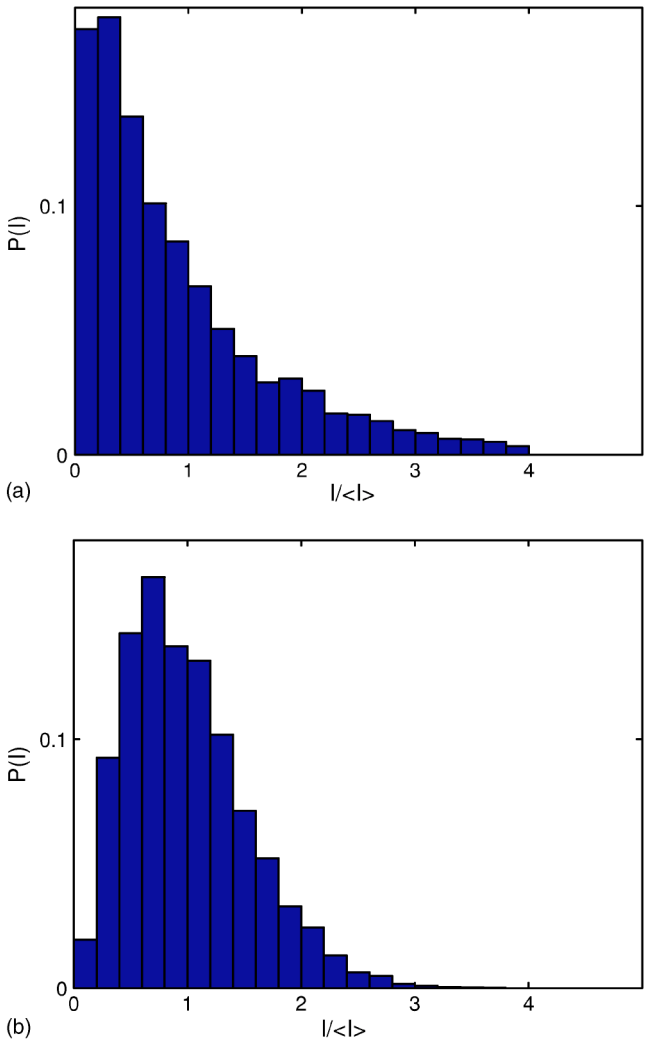

FIG. 2. Measured intensity distribution of the central signal mode of OPG versus the normalized intensity determined from 5000 pulses. (a) OPG operated at threshold energy. The signal intensity noise is 100%. (b) OPG pumped at 2 times the threshold energy. The relative signal intensity noise decreased to 54%.

profile. We focus on studying the statistical properties of the central (or on-axis) emission, which is a good representative of the full emission spectra. Since the central region is always the first one to be amplified, the pump threshold of the OPG is actually the threshold of the central mode. Figure 2(a) shows the intensity distribution of the central signal mode of our OPG operated at threshold; it is very close to a negative exponential function. Here 5000 pulses were used in the average. The noise level is 100%. Based on coherence properties of the SRS phenomenon [16], the exponential distribution that we find for the OPG intensity distribution is strong evidence that the central mode of the OPG is spatially coherent. This result is explained as follows. At threshold operation, only the small radial area at the center of the pump beam has enough gain to overcome other losses; the effective Fresnel number is small for this region, and hence the central mode has a single transverse mode.

For the OPG operated near the threshold, the signal is small and the pump is almost undepleted; near threshold, the amplification is in the linear regime, so the statistical properties of the initial field will be similar for different pump intensities. For the on-axis frequency with a single transverse mode, its initial field is generated from a Gaussian random distribution; thus, the intensity distribution of amplified signal is a Poisson distribution function of the intensity.

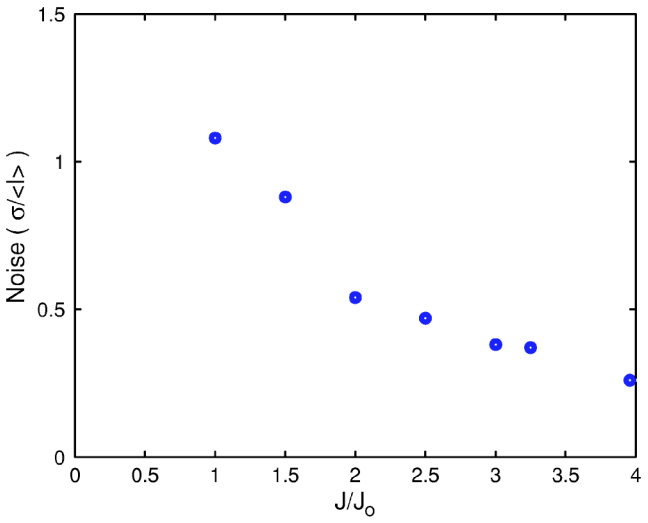

FIG. 3. Measured relative noise level of the central mode versus the ratio of the pump energy J to the threshold energy J_0.

As the pump energy per pulse is increased, the gain area becomes wider and the effective Fresnel number is larger. The emission statistics manifests spatial incoherence as multiple transverse modes begin to participate in the emission process. This is observed in the intensity distribution of the signal output, which deviates from the exponential function with its maximum moving toward the central mean intensity. Figure 2(b) is a plot of the central mode intensity distribution when OPG is operated at 2 times threshold pump energy; the relative signal intensity standard deveiation decreased to 54%.

Our results also show that as the gain increases, the noise, as measured by the relative standard deviation of the central signal-mode intensity, decreases. This is demonstrated in Fig. 3. For the OPG operated around 2 times the pump threshold, the relative noise level has decreased by about a factor of 2; increasing the pump energy further above 2 times threshold, the noise level is monotonically reduced. This is attributable to gain saturation of the central mode. As the peak pump intensity increases the signal is limited by the energy that can be extracted from the pump. So even though the signal has large intensity fluctuations after propagation through the medium its final value is clamped by the energy of the pump.

There are more frequencies amplified when the OPG is operated above threshold; these modes are uncorrelated except that they connect with each other by competing for pump energy and deplete its value. Each frequency mode also has its own multiple transverse modes, so the final OPG pulse can be temporally incoherent as well as spatially incoherent. The distribution of the total pulse intensity should look more like a Gaussian shape with higher distribution around the mean intensity; the noise of the total pulse intensity is lower than the noise of individual modes intensities.

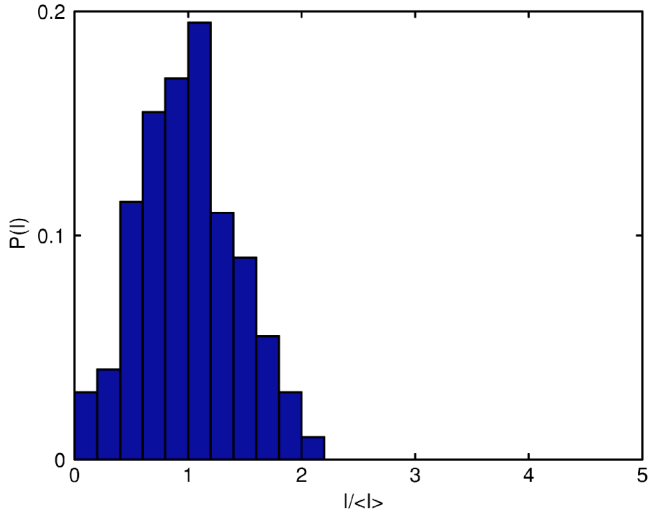

FIG. 4. Experimental result of the total pulse intensity distribution of the OPG pumped at 2 times threshold. The relative noise is 43%.

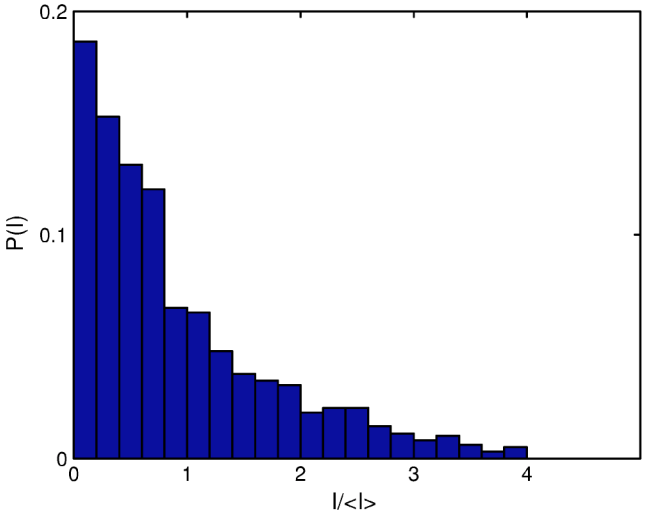

FIG. 5. The calculated intensity distribution of a single-mode output signal for undepleted pump determined from 500 runs.

Figure 4 shows the total pulse intensity distribution when the OPG is pumped at 2 times threshold. The total pulse intensity is slightly more stable, with a relative standard deviation of the intensity of 43%.

B. Numerical results

For simplicity, we start our analysis for an undepleted pump OPG. The analytic solution of the undepleted pump case with a constant pump profile is well known [26]:

$$A_s(z) = \left[A_s(0)\left(\cosh(gz) - \frac{i\Delta k}{2g} \sinh(gz) \right) + \frac{i\alpha_s}{g} A_i^*(0) \sinh(gz) \right] e^{i\Delta kz/2}, \tag{14}$$

$$A_i(z) = \left[A_i(0)\left(\cosh(gz) - \frac{i\Delta k}{2g} \sinh(gz) \right) + \frac{i\alpha_i}{g} A_s^*(0) \sinh(gz) \right] e^{i\Delta kz/2}, \tag{15}$$

where

$$\alpha_s = \frac{\omega_s \chi^{(2)} A_p}{2 n_s c}, \tag{16}$$

$$\alpha_i = \frac{\omega_i \chi^{(2)} A_p}{2 n_i c}, \tag{17}$$

$$g = \left[\alpha_s \alpha_i^* - \left(\frac{\Delta k}{2} \right)^2 \right]^{1/2}. \tag{18}$$

This solution is for a plane-wave field or a single mode; A_p is the amplitude of the undepleted pump wave, which is a constant. For the nonlinear coefficient we use the value $\chi^{(2)} = 34$ pm/V. We initiate the amplitude of signal and idler as Gaussian random values; the intensity distribution of output signal is an exponential function, as shown in Fig. 5. The noise level is around 100%.

For the depleted pump case, we numerically simulate the OPG process and examine the OPG pulse fluctuations for various pump intensities. For measured data, the mode spacing was determined by the spectrometer resolution, which is 0.07 nm. To keep the computation time manageable, we used a mode spacing of 0.5 nm in our calculations; the larger mode spacing did not affect our conclusions. The pump laser pulse energy fluctuation is accounted for by including 4% rms random fluctuations in our simulations. Figures 6(a), 6(c), and 6(e) are the calculated spectra of output signal when the OPG is pumped at threshold and 1.5 times and 2 times above threshold, respectively. Figures 6(b), 6(d), and 6(f) are the corresponding noise level plots of the individual modes. The on-axis modes are centered around 1482 ± 3 nm. The plots show the tendency toward higher fluctuations for the modes with off-axis phase matching angle, specifically for the operations above threshold.

For the OPG pumped at threshold, the intensity distribution of the on-axis phase-matched mode [see Fig. 7(a)] is very close to an exponential function and the relative noise level is around 150%; this result indicates that, at threshold operation, the on-axis mode has a monotransverse mode or spatial coherence. As we further increase the pump energy to 1.5 times and 2 times of the threshold, the central-mode intensity distribution deviates from a Poisson distribution function and moves toward a Gaussian distribution [see Figs. 7(b) and 7(c)]; the relative noise level decreases to 64% and 37%. This compares well with the experimental results reported in Fig. 2.

The plot in Fig. 8(a) shows the decreasing trend in the relative signal intensity noise for the central mode as the pump energy is increased. Figure 8(b) is a plot of the total pulse intensity distribution of the OPG operated at 1.5 times threshold; the distribution has a narrow peak around the mean intensity I_0. The relative standard deviation of total

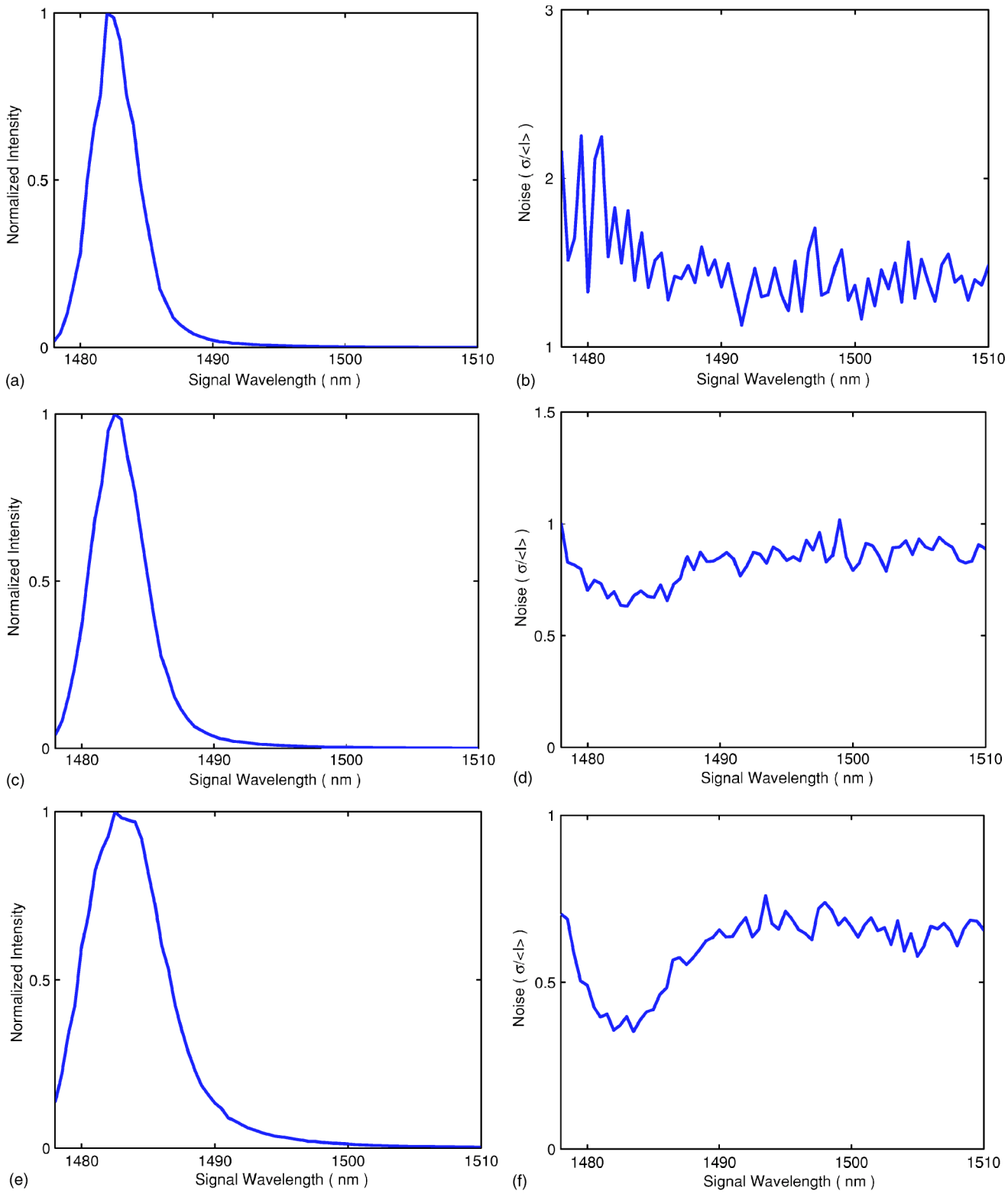

FIG. 6. Simulation results for the OPG calculated by averaging over 300 OPG pulses: (a), (c), and (e) mode spectrum of the signal wave for pump energies at threshold, 1.5 times threshold, and 2 times threshold, respectively, and (b), (d), and (f) relative noise level of individual modes when the OPG is pumped at threshold, 1.5 times threshold, and 2 times threshold, respectively.

pulse intensity is 45%. Again our simulations are in good agreement with experimental results reported in Fig. 3.

Our simulations show that the central mode is amplified first in the OPG process. As the pump pulse energy increases, more and more off-axis phase-matched modes are amplified and have a contribution to the output signal intensity. In other words, each individual mode is amplified at its own pump threshold level (the pump threshold we used in mea-

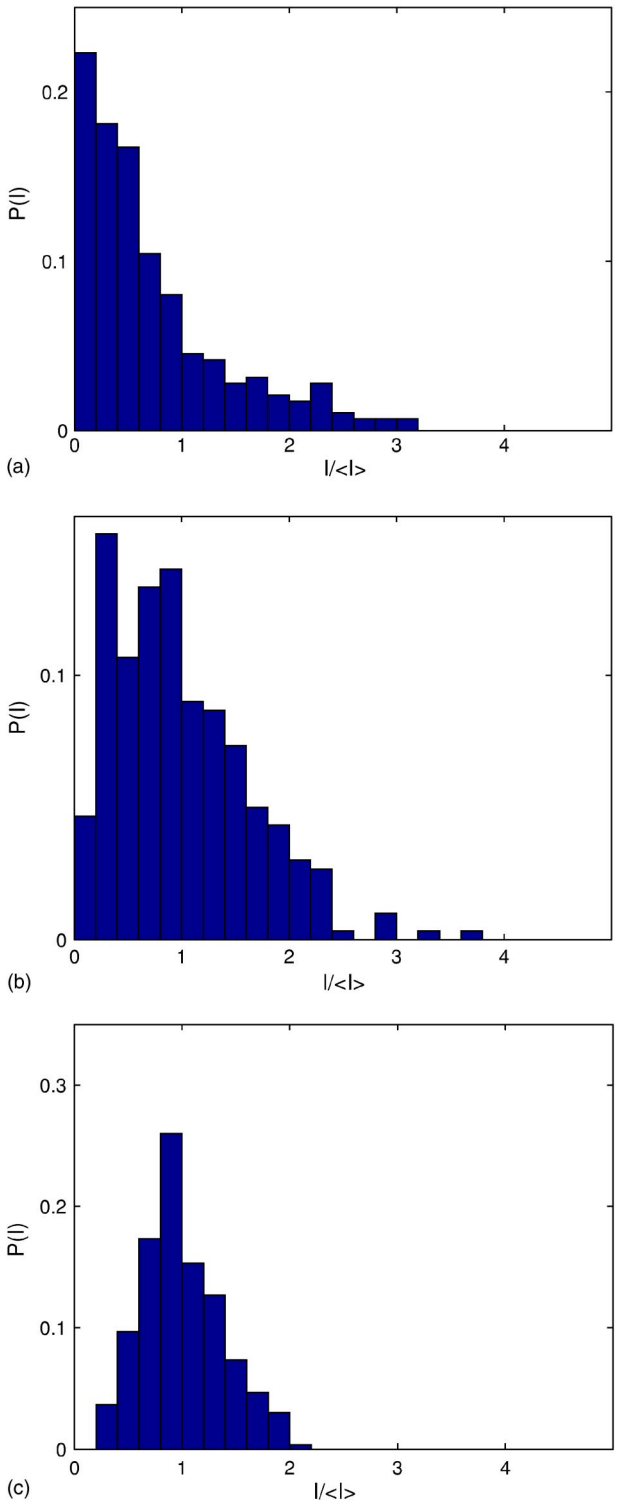

FIG. 7. The calculated central-mode intensity distribution of the OPG determined from 300 pulses: (a) the OPG operated at the threshold pump energy, (b) the OPG operated with the pump at 1.5 times threshold, and (c) the OPG operated with the pump at 2 times threshold.

surements and calculations actually is the threshold of the on-axis phase-matched mode). Off-axis modes have the same noise behavior as the on-axis mode; that is, the noise level decreases with increasing pump energy.

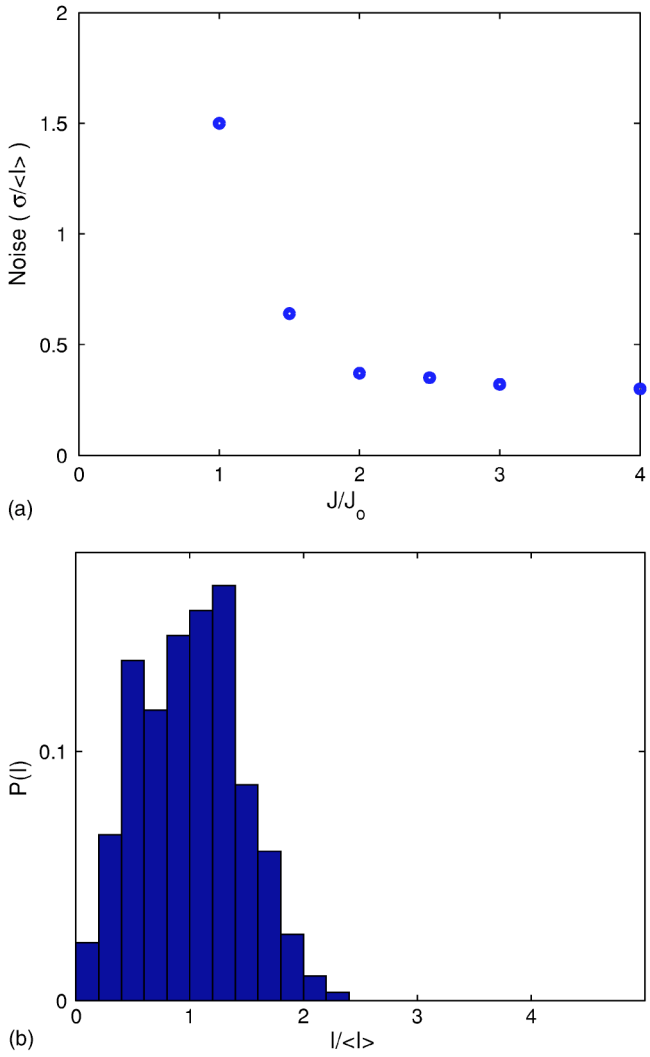

FIG. 8. (a) Calculated relative noise level of the central mode versus the ratio of the pump energy J to the threshold energy J_0 and (b) calculated result of the total pulse intensity distribution. The OPG operated at 1.5 times threshold.

Comparing our simulation results to the experimental results, the calculated central-mode relative noise level at threshold is 150%, which is higher than the measured one and higher than the analytic result for the single-mode undepleted pump. This is due to pump depletion effects even close to threshold. As previously mentioned in the experiment we define a threshold pump level when the output signal is detectable, which is actually the central-mode threshold. In that case the OPG process is still in the undepleted pump region.

However, in the calculations, the threshold pump level is defined as the knee in the curve of the total signal intensity versus pump intensity. This definition is similar to the lasing threshold; below threshold the output is very small and above threshold the signal intensity versus pump intensity is linear. The threshold point is at the knee in the curve between the two regions. In our previous paper [29], we found that the off-axis modes begin to appear when the central mode starts to be backconverted to the pump. In the other words,

before the off-axis modes are measured, the output is still a single mode (central mode), but the process is in the depleted pump region.

For the depleted pump, the macroscopic quantum fluctuations are not just the linear amplification of the initial quantum noise. To understand the affect of pump depletion, we also simulate the single-mode, depleted pump process and find that the distribution function of signal power is distorted from the exponential function; the relative noise level is greater than 100%. This result demonstrates the difference between the two definitions of the threshold; the threshold pump level used in calculations is higher than the one used in the experiment. For the same reason, the calculated results at 1.5 times threshold are close to the measured results of 2 times threshold. This correspondence is clearly observed by comparing between the experimental results and the simulations—i.e., Figs. 1(a) and 1(b) with Figs. 6(c) and 6(d), Fig. 2(b) with Fig. 7(b), and Fig. 4 with Fig. 8.

In addition, the experimental pump laser pulse energy fluctuations were in the range 4%–6% in our measurements, which could enhance the macroscopic fluctuations of OPG pulses, particularly for the OPG operated at low pump energy levels. This is another reason why our simulation calculations have a smaller noise level for signal fluctuations in the on-axis regime when operated above threshold compared to the experimental results. So the discrepancy of the threshold and pump fluctuations between the simulations and the measurements results in the discrepancy of calculated and experimental results; however, our simulations predict the right trend for the statistical behavior of the OPG.

The third cause for the discrepancy between our calculations and experiments is the assumption that the pump pulse is a Gaussian function of time. The experimental pulses may be more complex than a simple Gaussian function, and their shape could change from shot to shot. This is not measurable with our experimental setup.

IV. CONCLUSION

We used a 3-cm-long PPLN crystal to experimentally measure the statistical properties of the signal emission from a nanosecond-pumped QPM OPG. A model is presented that has been successful in describing off-axis broadband emission processes in the OPG [29]. Simulations of quantum noise using this model show good agreement with the experimental results. We focused on studying the signal emitted along the central axis because it was the dominant contribution for the QPM OPG, and its behavior was representative of the other individual signal emissions.

When our OPG was operated close to threshold, the on-axis signal-mode intensity distribution was close to an exponential function, which indicated that only the signal close the central axis was amplified and it was spatially coherent. By increasing the pump energy above the threshold, the on-axis emission became spatially incoherent and at the same time off-axis signal reached threshold and contributed to the overall emission. The signal output from the OPG was temporally and spatially incoherent, but the fluctuations in the total pulse intensity were much lower than the fluctuations of the pulse intensity of the individual modes. The noise of the on-axis intensity decreased with increasing pump energy; also the on-axis signal had the lowest fluctuations among all the individual emissions, including off-axis contributions. A numerical model was used to simulate the quantum initiation and signal amplification of the QPM OPG process, which accurately predicts the statistical properties of the on-axis signal intensity fluctuations.

ACKNOWLEDGMENTS

This work is partially supported by NSF Grant No. ECS-0140109. Y.G. was supported by a DAGSI grant from the State of Ohio.

[1] W. H. Louisell, A. Yariv, and A. E. Siegman, Phys. Rev. **124**, 1646 (1961).
[2] R. Graham and H. Haken, Z. Phys. **210**, 276 (1968).
[3] A. S. Lane, M. D. Reid, and D. F. Walls, Phys. Rev. A **38**, 788 (1988).
[4] T. Schroder, K.-J. Boller, A. Fix, and R. Wallenstein, Appl. Phys. B: Lasers Opt. **58**, 425 (1994).
[5] A. Fix and R. Wallenstein, J. Opt. Soc. Am. B **13**, 2484 (1996).
[6] G. Arisholm, J. Opt. Soc. Am. B **16**, 117 (1999).
[7] L. Mandel and E. Wolf, *Optical Coherence and Quantum Optics* (Cambridge University Press, Cambridge, England, 1995).
[8] M. Beck, C. Dorrer, and I. A. Walmsley, Phys. Rev. Lett. **87**, 253601 (2001).
[9] F. Haake, H. King, G. Schroeder, J. W. Haus, R. Glauber, and F. Hopf, Phys. Rev. Lett. **42**, 1740 (1979).
[10] Q. H. F. Vrehen and J. J. der Weduwe, J. Opt. Soc. Am. **70**, 610 (1980).
[11] P. Kravis and L. Allen, Opt. Commun. **23**, 289 (1977).
[12] I. A. Walmsley and M. G. Raymer, Phys. Rev. Lett. **50**, 962 (1983).
[13] M. Scalora, C. M. Bowden, and J. W. Haus, Phys. Rev. Lett. **69**, 3310 (1992).
[14] M. Scalora and J. W. Haus, Opt. Commun. **87**, 267 (1992).
[15] I. A. Walmsley and M. G. Raymer, Phys. Rev. A **33**, 382 (1986).
[16] I. A. Walmsley, M. G. Raymer, J. Mostowski, and B. Sobolewska, Phys. Rev. A **32**, 332 (1985).
[17] H. A. Haus and S. Kawakami, IEEE J. Quantum Electron. **21**, 63 (1985).
[18] I. H. Deutsch, J. C. Garrison, and E. M. Wright, J. Opt. Soc. Am. B **8**, 1244 (1991).
[19] S. J. Kuo, D. T. Smithey, and M. G. Raymer, Phys. Rev. A **45**, 2031 (1992).
[20] M. J. Missey, V. Dominic, P. E. Powers, and K. L. Schepler, Opt. Lett. **25**, 248 (2000).
[21] G. Hansson and D. D. Smith, Opt. Lett. **25**, 1783 (2000).
[22] S. Haidar, T. Usami, J. Shikata, and H. Ito, Opt. Eng.

(Bellingham) **42**, 143 (2003).
[23] T. A. Reichardt, R. P. Bambha, T. J. Kulp, and R. L. Schmitt, Appl. Opt. **42**, 3564 (2003).
[24] J. J. Zayhowski, Opt. Lett. **22**, 169 (1997).
[25] P. E. Powers, K. W. Aniolek, T. J. Kulp, B. R. Richman, and S. E. Bisson, Opt. Lett. **23**, 1186 (1998).
[26] Robert W. Boyd, *Nonlinear Optics* (Academic, Boston, 1992).
[27] J. W. Haus, Y. Guan, and P. E. Powers, Proc. SPIE **5337**, 60 (2004).
[28] S. M. Russell, P. E. Powers, M. J. Missey, and K. L. Schepler, IEEE J. Quantum Electron. **37**, 877 (2001).
[29] Y. Guan, J. W. Haus, and P. E. Powers, J. Opt. Soc. Am. B **21**, 1225 (2004).